Review Article

Biochar Microparticles from Pomegranate Peel Waste: Literature Review and Experiments in Isotherm Adsorption of Ammonia

Asep Bayu Dani Nandiyanto*, Adisti Eka Putri, Meli Fiandini and Risti Ragadhita
Universitas Pendidikan Indonesia, Bandung, Indonesia

Teguh Kurniawan
Teknik Kimia, Fakultas Teknik, Universitas Sultan Ageng Tirtayasa, Banten, Indonesia

* Corresponding author. E-mail: nandiyanto@upi.edu DOI: 10.14416/j.asep.2024.08.009
Received: 11 April 2024; Revised: 11 June 2024; Accepted: 17 July 2024; Published online: 19 August 2024

Abstract
This research aimed to synthesize biochar microparticles from pomegranate peel waste for ammonia adsorption. This research also focused on analyzing adsorption isotherm and kinetics models to understand the mechanism of ammonia adsorption on the biochar. The experiments were conducted by carbonizing pomegranate peel waste. The carbonized material was then milled and sieved to obtain biochar microparticles with a certain size (i.e. 500, 1000, and 2000 μm). The particles were then characterized using microscopy and infrared spectroscopy (FTIR) to identify particle morphology and functional groups. The prepared particles were then used for the ammonium adsorption process, and compared with ten isotherm models (such as Langmuir, Freundlich, Temkin, Dubinin-Radushkevich, Jovanovic, Halsey, Harkin-Jura, Flory-Huggins, Fowler-Guggenheim, and Hill-Deboer) to identify the adsorption mechanism. Adsorption kinetic analysis was also performed to identify the adsorption rate of the prepared particles using first-order and second-order pseudo-kinetic models. The adsorption isotherm model informed that ammonia adsorption on biochar with sizes of 2000 μm (large) and 1000 μm (medium) occurs in a multilayer process with physical interaction accompanied by pore filling. Meanwhile, small biochar (500 μm) indicates that the ammonia adsorption process occurs on homogeneous sites with physical interaction through pore filling. From the results of fitting the isotherm model, information about the maximum adsorption capacity for each size of 2000, 1000, and 500 μm are 65.631, 62.231, and 50.086 mg/g, respectively. Overall, the adsorption mechanism occurring on biochar involves interactions among ammonia molecules that repel each other under endothermic conditions. The largest adsorption capacity was obtained for biochar with sizes of 2000 μm. Analysis of adsorption kinetics showed that the adsorption process follows a first-order pseudo-kinetic model, indicating an adsorption mechanism controlled by intraparticle diffusion. This study concludes that biochar from pomegranate peel is prospective for use as an environmentally friendly adsorbent for ammonia removal applications from wastewater, offering a sustainable and effective alternative adsorbent to existing water treatment technologies and solving current issues in the sustainable development goals (SDGs).

Keywords: Adsorbent, Adsorption kinetic, Ammonia, Biochar, Isotherm models, Pomegranate peel

1 Introduction

Biochar is a solid material formed through the pyrolysis process of biomass. It results in a solid that is rich in carbon. Biochar has several unique physicochemical characteristics, making it very useful for various environmental applications [1]. Biochar is similar to carbon in terms of its physicochemical characteristics, such as 1) porous structure (mainly a combination of micropores and hierarchical pores), 2) rich in functional groups (mainly oxygen-containing component), 3) high degree of aromatic structure, and 4) large specific surface area [2]–[4]. Some of the physicochemical characteristics previously mentioned

allow biochar to have a high adsorption capacity, making biochar capable of binding various types of contaminants such as heavy metals, organic compounds, and inorganic compounds that accumulate in water [1]. Due to its great potential in the field of adsorption, research interest in this material is increasing significantly. Figure 1 shows research trend data related to research with the keywords "biochar" and "adsorption" taken from the Scopus database as of 8 June 2024. Figure 1 reveals that biochar-related research has consistently increased each year as indicated by the increase in the number of documents related to such research per year, reflecting the growing interest of the scientific community in the potential biochar in adsorption applications. This trend also indicates an increased awareness of biochar's ability as an effective adsorbent material for wastewater treatment, environmental remediation, and pollution abatement.

Existing research on conventional methods for biochar production, including various production methods, preparation conditions, and yields are summarized in Table 1. Indeed, biochar products can be produced from various conventional methods. Based on the literature, the thermal carbonization production method is one of the popular production methods to produce biochar. The product is also suitable for pollutant adsorption applications in aqueous media. The method has an advantage since it does not produce secondary by-products. However, it has limitations due to the high cost and time-consuming process [5]. Other methods (such as slow pyrolysis, fast pyrolysis, and flash pyrolysis) have been suggested, only producing relatively few main products (<50%). In addition, gasification methods are also generally only used for the production of gas materials (biogas), leading to more product content (in the gas phase) than biochar products over time [1], [6].

Table 2 shows several studies that have been carried out to identify knowledge gaps regarding the selection of production methods and raw materials to obtain biochar properties and meet the requirements of adsorption applications [7]–[14]. Although there is much interest in using biochar in adsorption applications, there is still an information gap about biochar properties that must be bridged to promote successful biochar utilization. Based on existing studies (Table 2), current research presents gaps regarding 1) biochar production with different biomasses; 2) the use of simple biochar production methods at low temperatures to produce macro-micro pore distribution; thus, saving energy and providing knowledge about simple ways to manage and utilize organic waste; 3) the use of thermal carbonization methods for high-yield biochar production; 4) biochar production without the addition of other chemicals; and 5) the interaction mechanism of biochar with varying sizes during the adsorption process. Also, there is no research on the use of pomegranate peel as raw material for adsorption, as well as explaining phenomena during the adsorption of ammonium in solution using the prepared biochar from this raw material.

The objective of this research is to prepare biochar from pomegranate peel (*Punica granatum* L.) with various specific particle sizes (i.e., 500, 1000, and 2000 μm) for water contaminant removal applications.

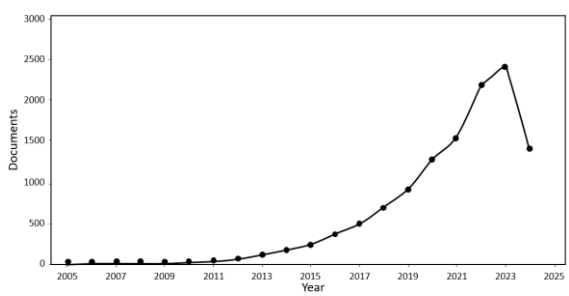

Figure 1: Research trends of "biochar" and "adsorption" from year to year (taken from www.scopus.com; on 8 June 2024. Detailed information for the use of bibliometrics is explained elsewhere [15].

Table 1: Conventional methods of biochar production [1].

Method	Temperature (°C)	Reaction Time	Yield (%)		
			Solid	Liquid	Gas
Slow Pyrolysis	<700	h	35	30	35
Fast Pyrolysis	<1000	s	10	70	20
Flash Pyrolysis	775–1025	s	10–15	70–80	5–20
Carbonization Thermal	<350	min to h	50–80	-	-
Gasification	700–1500	s to min	10	5	85

The scientific issues that are the focus of this study include an in-depth understanding of adsorption mechanisms and adsorption kinetics to predict biochar performance. In addition, this research is concerned with exploring how particle size affects adsorption effectiveness. Here, pomegranate peel-based biochar was produced via a thermal carbonization method as carried out in previous research [16]–[25]. Previous research has shown that various types of agricultural waste can be utilized as biochar through thermal carbonization as shown in Table 3, in which the methods were adopted to support the present production of biochar from pomegranate peel. The rationalized thermal carbonization production method was selected in this study because it produces relatively high biochar products and does not produce secondary products. Furthermore, the biochar particles that have been produced are characterized using a microscope and infrared spectroscopy (FTIR) to identify the particle morphology and respective functional groups, respectively. Then, the prepared particles were used for the ammonia adsorption process, tested, and compared with ten isotherm models (such as Langmuir, Freundlich, Temkin, Dubinin-Radushkevich, Jovanovic, Halseys, Harkin-Jura, Flory-Huggins, Fowler-Guggenheim, and Hill - Deboer) to identify the adsorption mechanism.

Pomegranate fruit was selected as a raw material for the present biochar production because this fruit is one of the popular fruits in Indonesia (see https://repository.penerbiteureka.com/tr/publications/563614/mengenal-lebih-dekat-delima-buah-surga-kaya-manfaat). It is rich in organic content as a carbon source. The organic component contained in pomegranates is around 33–62% which mainly consists of lignin and cellulose as carbon sources which are the main components of biochar [26].

In this study, we also focused on the analysis of adsorption of the biocar for adsorbing ammonia as a model adsorbate. Ammonia is an inorganic compound that may accumulate in water. Ammonia (NH_3) in water is usually found in the form of ammonium (NH_4^+), which is the result of decomposition of organic materials or industrial waste (such as textile, leather, paper, printing, and cosmetics industries) [27]–[29]. Ammonium is a form of nitrogen that can cause eutrophication in water bodies, resulting in excessive algae growth and decreased water quality [30]–[32]. Increasing ammonium concentrations in water can also be a threat to human health and aquatic ecosystems, thus managing and reducing ammonium concentrations in wastewater is very important. Therefore, there is a need for serious, comprehensive, and sustainable solutions to solve this problem. Solving this issue also helps the sustainable development goals (SDGs), while SDGs are now being taught to society [33]–[35].

This study provides new information related to the fabrication of environmentally friendly adsorbents to remove ammonia pollutants by utilizing pomegranate peel-based biochar. These findings suggest that biochar from pomegranate peel waste can be an effective and sustainable alternative for wastewater treatment, offering an eco-friendly solution by utilizing abundant organic waste. Thus, this research not only adds insight into the use of biochar as an ammonia adsorbent but also encourages the application of green technology in wastewater pollutant management.

Table 2: Current progress in biochar production for the adsorption process.

Production Method	Raw Material / Adsorbate	Advantages	Disadvantages	Ref.
Pyrolysis	Algae / Ciprofloxacin	• Biochar was produced at low temperatures (< 150 °C). • Biochar from algal raw material had a mesoporous structure, playing a role in increasing the specific surface area and increasing accessibility to target molecules for being absorbed. • Renewable energy source through biomass pyrolysis.	• Biochar was modified by adding a chemical activator ($ZnCl_2$) causing it to become environmentally unfriendly. • Adsorption isotherm studies were not discussed comprehensively. • There had been no quantitative comparison of the influences of different functional groups. • There was no illustration of the possible adsorption mechanisms that occur.	[7]

Table 2 (*Continued*).

Production Method	Raw Material / Adsorbate	Advantages	Disadvantages	Ref.
Pyrolysis	Bamboo Clum / Atrazine	• Biochar was successfully produced at different temperature conditions (namely 350, 450, and 550 °C). • Biochar with a production temperature above 500 °C had a micro-mesoporous structure, contributing significantly to the adsorption process. • The biochar produced was environmentally friendly because it does not use other chemical additives.	• Biochar produced below 500 °C had a disorganized structure and a smaller micropore volume resulting in a small specific surface area, which contributes to the ineffectiveness of the adsorption process. • The best-performing product was biochar produced at high temperatures (>550 °C). The biochar production process at high temperatures requires significant energy consumption, especially to achieve high temperatures and maintain proper process conditions. Therefore, in terms of energy efficiency, biochar production at high temperatures might not be optimal. • Adsorption isotherm studies were not discussed comprehensively. • There was no illustration of the possible adsorption mechanisms that occur.	[8]
Microwave pyrolysis	Wheat straw / Heavy Metal	• Biochar was produced via the microwave method to heat organic materials at certain power variations (100, 200, 300, 400, 500, and 600 W), which could be controlled well and was usually faster than other conventional methods. • Biochar prepared with higher microwave power was much coarser and had more debris and holes, which might provide more potential adsorption sites for heavy metals. • Biochar production did not involve additional chemicals. • Microwave biochar from higher power levels (400–600 W) showed better reusability and maximum adsorption efficiency.	• The yield of the products produced was relatively low (20–40%). • Adsorption isotherm studies were not discussed comprehensively. • Although biochar produced by microwaves at these higher power levels showed good performance, this production method could be considered energy inefficient compared to other production methods, such as conventional pyrolysis or thermal carbonization. • There was no illustration of the possible adsorption mechanisms that occur.	[9]
Pyrolysis	Watermelon seeds / Heavy metal	• Biochar was produced from production methods at low temperatures (<400 °C) thereby saving energy.	• Biochar was modified by adding the chemical hydrogen peroxide which causes biochar to become environmentally unfriendly. • Unmodified biochar had a low pore structure, resulting in low adsorption capacity. • Further research was still needed to develop new low-cost and high-efficiency biochar modification technologies to improve the practical application of the resulting adsorbent materials in wastewater treatment.	[10]
Pyrolysis	Ragweed (*Ambrosia artemisiifolia L.*) and Horseweed (*Conyza canadensis L.)* / Heavy Metal	• Biochar production was successfully carried out at temperatures of 350, 450, and 550 °C. • The production process was carried out without the addition of chemicals. • Biochar produced at temperatures of 450 and 550 °C had a mesoporous structure. • Biochar was produced without the addition of other chemicals.	• Biochar produced at temperatures lower than 550 °C had low adsorption capacity due to its low specific surface area. • The best-performing material is biochar produced at high temperatures. However, the use of high temperatures requires significant energy consumption. • Adsorption isotherm studies were not discussed comprehensively.	[11]

Table 2 (*Continued*).

Production Method	Raw Material / Adsorbate	Advantages	Disadvantages	Ref.
		• Biochar had a high adsorption capacity (>100 mg/g for the heavy metal Cd^{2+} and >300 mg/g for the heavy metal Pb^{2+}).	• There was no illustration of the possible adsorption mechanisms that occur.	
Pyrolysis	Loofah fiber / 4-Nitrophenol	• Loofah-based biochar was successfully prepared at relatively low temperatures (below 400 °C). • Biochar had an aligned microchannel structure with a diameter of about 10 μm and was porous. • The resulting structure could provide a large enough surface area and facilitate the adsorption of 4 nitrophenols through the pore-filling process. • A schematic illustration of the adsorption mechanism was presented.	• The addition of other chemicals in the biochar production process made the material environmentally unfriendly. • A two-step activation process needed to be carried out to obtain a biochar product with good performance.	[12]
Pyrolysis	Grape Pomace / Heavy Metal	• Biochar was successfully produced at temperatures of 300, 500, and 700 °C. • It needed a short production time (2 h). • Biochar is produced without the addition of chemicals.	• Greater product yield was produced when production was carried out at high temperatures. The use of high temperatures requires significant energy consumption. • Biochar at low temperatures did not provide good adsorption performance. • The best-performing product was biochar produced at high temperatures. However, the use of high temperatures requires significant energy consumption.	[13]
Pyrolysis	Elephant grass / Violet dye	• Biochar was successfully produced at temperatures of 350, 600, and 900 °C without the addition of chemicals. • Biochar was produced at higher pyrolysis temperatures, especially 900 °C, exhibiting a greater number of pores, compared to biochar produced at 350 °C. • In most cases, except for products produced at low temperatures, the removal efficiency did not change substantially, indicating a good ability to reuse materials in continuous flow adsorption.	• Yield of biochar produced was less than 50%. • Biochar retained the morphological characteristics of biomass in nature. • The surface area increases with increasing pyrolysis temperature and residence time. Therefore, at the same temperature, biochar produced with a longer residence time produced a larger surface area. The use of higher temperatures and longer residence times can also increase energy consumption significantly.	[14]

Table 3: Previous research related to processing biomass waste using the thermal carbonization method for adsorption applications.

Raw Material	Adsorbate Model	Results	Ref.
Mangosteen Peel	Curcumin	• Biochar with certain particle sizes (i.e., 500, 1000, 2000 μm) had an adsorption capacity of 500.570, 333.330, and 244.450 mg/g respectively. • The adsorption mechanism for small-sized adsorbents (500 μm) followed the Langmuir and Harkin Jura isotherms, meaning a physical adsorption mechanism with monolayer formation and pore filling. • The adsorption mechanism for large-sized adsorbents (1000 and 2000 μm) followed the Hill-Deboer, Flory Huggins, and Fowler Guggenheim isotherms, meaning a physical adsorption mechanism with multilayer formation and pore filling.	[16]
Rice Husk	Curcumin	• Biochar with certain particle size variations (i.e., 500, 177, and 74 μm) had an adsorption capacity of 681.40, 361.48, and 687.40 mg/g, respectively. • The small particle followed the adsorption mechanism of multilayer formation without pore filling, following the isotherm model of Jovanovic, Fowler Guggenheim, Temkin, Freundlich Halsey, Flory Huggins, Harkin Jura, Hill-Deboer, Langmuir and Dubinin-Radushkevich.	[17]

Table 3 (*Continued*).

Raw Material	Adsorbate Model	Results	Ref.
		• Large and medium particle sizes followed the adsorption mechanism of multilayer formation with pore-filling phenomena, following the isotherm models: Fowler Guggenheim, Jovanovic, Temkin, Hill-de Boer, Freundlich, Flory Huggins, Halsey, Dubinin-Radushkevich, and Langmuir.	
Tamarind Seed	Curcumin	• The adsorption capacity of each biochar particle size was 76.335 mg/g (2000 μm), 588.235 (1000 μm), and 78.125 (500 μm). The larger particles correlated to the more adsorption capacity. The optimal biochar particle size for the adsorption process was 1000 μm. • The adsorption mechanism for small-sized biochar followed the Halsey, Jovanovic, Harkin Jura, Temkin, Dubinin Radushkevich, and Langmuir isotherms with mechanisms of monolayer formation, physical interactions, pore filling, and cooperative type. • The adsorption mechanism for large-sized biochar followed the Alsey, Jovanovic, Harkin Jura, Temkin, Hill Deboer, Dubinin Radushkevich, and Langmuir isotherm with the mechanism involved being multilayer formation with a combination of physical and chemical interactions.	[18]
Jackfruit	Curcumin	• The appropriate isotherm model was the Jovanovic, Temkin, and Dubinin-Radushkevich isotherm models. • The adsorption mechanism followed physisorption interactions on a microporous homogeneous surface.	[19]
Mango Seed	Curcumin	• The results of adsorption studies were in good agreement with several models such as Jovanovic, Freundlich, Halsey, and Dubinin Radushkevich. • The adsorption mechanism was endothermic, spontaneous, and multilayer formation with a combination of physisorption and chemisorption interactions.	[20]
Avocado Seed	Curcumin	• The adsorption isotherm model was the Langmuir and Hill-Deboer model, meaning that the adsorption mechanism involved multilayers with physisorption interactions. • In addition, another model was the Temkin and Dubinin Radushkevich isotherm model, validating the cooperative mechanism with pore filling.	[21]
Date Palm Seed	Curcumin	• Biochar based on date seeds with varying particle sizes was successfully prepared. In this study, the biochar particle sizes evaluated in adsorption studies were 500, 250, and 100 μm. The smaller particles created better adsorption efficiency (reaching 53.44%) compared to other larger particles. • The adsorption isotherm results show a match with the Langmuir > Dubinin-Radushkevich > Jovanovic > Freundlich > Halsey isotherm, meaning that adsorption was normal, spontaneous, favorable, forming monolayers and multilayers on heterogeneous surfaces.	[22]
Papaya Seed	Curcumin	• One of the parameters influencing the adsorption process was particle size. Adsorbents with particle sizes of 500, 1000, and 2000 μm were successfully evaluated. • The small-size adsorbent had the best adsorption capacity. • The adsorption mechanism for small and medium particle sizes was the formation of a monolayer with adsorbent-adsorbate interactions occurring physically. • The large particle followed the adsorption mechanism of monolayer formation with adsorbent-adsorbate interactions occurring repulsively.	[23]
Pumpkin Seed	Curcumin	• Pumpkin seed-based biochar with varying sizes was successfully prepared. However, the adsorption capacity of pumpkin seed-based biochar was relatively low compared to other materials. The evaluation results show that the adsorption capacity of pumpkin seed-based biochar is < 50 mg/g. • The isotherm model shows that the adsorption process occurs physically through multilayer formation and pore filling which occurs spontaneously and favorably.	[24]
Pineapple Peel	Curcumin	• Carbon-based adsorbents were successfully prepared with size variations of 100, 125, and 200 μm. • The adsorption efficiency of each particle size is 83.08% (100 μm), 94.45% (125 μm), and 77.99% (200 μm), showing that the relatively smaller particle size indicates a better adsorption process than the smaller particle size. large particles. This is because the small particle size implies an increase in surface area. • Overall, adsorption follows a normal adsorption mechanism with physical interactions on the multilayer surface.	[25]

2 Method

2.1 *Materials and apparatuses*

The main material used in this research was pomegranate peel waste obtained from the local market in Indonesia. The other chemicals used include H_3PO_4 and pro-analysis grade of NaOH (obtained from E-Merck, Germany) and distilled water.

We also used analytical balance with an accuracy of 0.001 g (Ohaus PA214), an electrical furnace (Vulcan A-550), a digital microscope, a magnetic stirrer, an ammonia kit, and an Infrared Spectrophotometer (FTIR).

2.2 *Preparation of biochar microparticles from pomegranate peel waste*

In the experiment (Figure 2), the pomegranate peel waste was washed using running water and dried in the sun. After drying, the pomegranate peels were ground into small pieces using a mortar and pestle. Then, the pomegranate peels that have become smaller pieces are dried again using an electrical furnace at 220 °C for 4 h gradually until the pomegranate peels become black particles (biochar produced). The biochar was then milled and placed in the ASTM D1921 sieve shaker apparatus (Niaga Kusuma Lestari, Indonesia) to obtain a specific and homogeneous size (i.e. 500, 1000, and 2000 µm). Detailed information regarding the milling process is reported elsewhere [36].

In short, the sieve shaker was equipped with pans with hole sizes of 55, 74, 100, 125, 200, 500, 1000, and 2000 µm. The prepared biochar particles were then washed with ultrapure water and cleaned from their impurities using centrifugation (TG16WS; High-Speed Benchtop Centrifuge, Zhengzhou Hepo International Trading, Co., Ltd., China; 11,000 rpm for 5 min). Prior to using in the adsorption, the biochar adsorbent was dried in an electrical furnace at the temperature of 200 °C to remove the physically adsorbed water for 1 h. Detailed information for the fabrication process of biochar microparticles from pomegranate peel waste is presented in Figure 2. Adsorbent material fabrication uses the same method as reported in the literature [16]–[25].

2.3 *Surface activation of biochar adsorbent-based pomegranate peel*

To improve the quality of the adsorbent, surface activation was done [37]. The samples were then impregnated with 30% H_3PO_4 (a ratio of biochar/H_3PO_4 = 1:5) for 24 h. The impregnated sample was dried in an electrical furnace at 110 °C. Next, the dried impregnated biochar was activated at 700 °C for 1 h using an electrical furnace and neutralized by adding 1% NaOH to pH = 7. Then, the biochar was rinsed with distilled water to remove the salt formed and re-dried using an electrical furnace at 80 °C.

2.4 *Physicochemical characterization of prepared adsorbent*

Physical characterization relating to morphological examination for particle size evaluation was done using a Digital Microscope (BXAW-AX-BC, China). Meanwhile, chemical characterization relating to the identification of functional groups was done using Fourier Transform Infrared (FTIR) analysis using FTIR-4600 equipment from Jasco Corp, Japan.

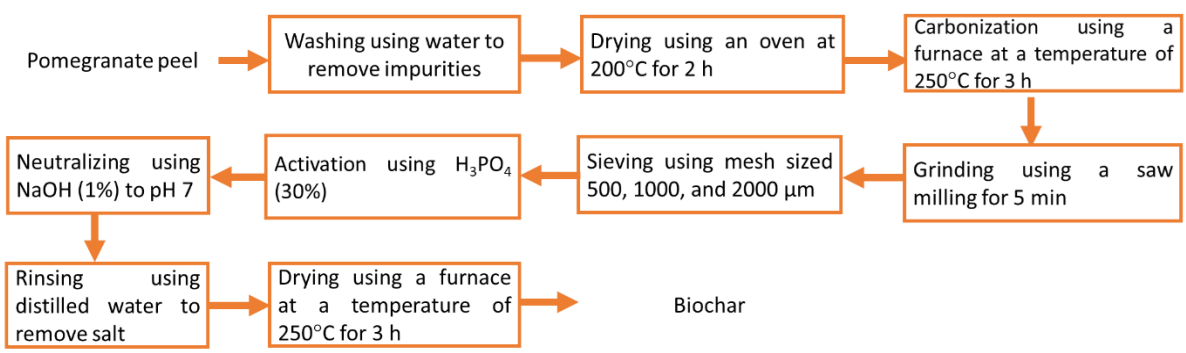

Figure 2: Flowchart of fabrication biochar from pomegranate peel. This process flow diagram is adopted and modified from previous studies [16]–[25].

2.5 *Adsorption procedure*

The adsorption was done in the batch reactor. The adsorbate was 100 mL of ammonia solution with various concentrations (i.e. 10, 20, 40, 60, and 80 ppm). In short, 100 ppm ammonia solution was prepared by dissolving 0.48 g of NH_4Cl in 0.5 L ultrapure water. To ensure the soluble concentration of ammonia, the concentration of ammonia solution was analyzed using the calorimeter method (Hanna HI733). In the experiment, the ammonia solution containing the biochar adsorbent was shaken manually and aged for 24 h at room temperature. The change in ammonia concentration was analyzed using using the calorimeter method (Hanna HI733).

To analyze the adsorption mechanism comprehensively, the adsorption data was interpreted and compared using ten isotherm models. To transmit the adsorption mechanism comprehensively, the adsorption data is interpreted using ten adsorption isotherm models (such as Langmuir, Freundlich, Temkin, Dubinin-Radushkevich, Jovanovic, Halseys, Harkin-Jura, Flory-Huggins, Fowler-Guggenheim, and Hill-Deboer). A brief overview of the theory of the ten isotherm models of adsorption is explained as follows [38]:

2.5.1 Langmuir

The Langmuir isotherm model explains that the formation of a single layer on the surface of the adsorbent indicates a maximum adsorption process. The Langmuir model posits that there is no migratory movement of adsorbate molecules, and adsorption exclusively occurs on a stationary surface that has a uniform energy distribution. The Langmuir isotherm expression is anticipated using Equations (1) and (2).

$$\frac{1}{Qe} = \frac{1}{Qmax\ KL}\ \frac{1}{Ce} + \frac{1}{Qmax} \quad (1)$$

$$RL = \frac{1}{1+KL\ Ce} \quad (2)$$

where q_{max} is the Langmuir equilibrium constant and is the maximal monolayer capacity (mg/g). The following K_L is the Langmuir-Vagelar equation. In addition, R_L describes unfavorable adsorption ($R_L > 1$); linear adsorption (affected by the amount and concentration of adsorbed molecules) ($R_L = 1$); too strong adsorption or irreversible adsorption ($R_L = 0$); and favorable adsorption or no desorption ($0 < R_L < 1$).

2.5.2 Freundlich

This model describes a type of physical adsorption in which the adsorption occurs in multiple layers, and the bonds are weak (multilayer). The Freundlich isotherm also explains the degree of linearity (n) between the adsorbate solution and the adsorption process, which is described as follows: $n = 1$, linear adsorption; $n < 1$, adsorption process with chemical interaction; $n > 1$, adsorption process with physical interaction; Favorable adsorption process is declared when $0 < \frac{1}{n} < 1$, and a cooperative adsorption process occurs when $\frac{1}{n} > 1$. The isotherm model can be expressed using Equation (3).

$$\log Qe = \log kf + \frac{1}{n}\log Ce \quad (3)$$

where kf is the Freundlich constant; Ce is the equilibrium adsorbate concentration (mg/L); and $1/n$ signifies the adsorption strength

2.5.3 Temkin

In line with the Temkin isotherm model, there is a linear decline in the adsorption heat of all molecules as the adsorbent surface coverage expands. Equation (4) serves as the tool for calculating the adsorption heat for all molecules within the multilayer.

$$qe = \beta T\ (\ln Ce) + (BTlnAT) \quad (4)$$

The equilibrium constant for the Temkin isotherm model is denoted as A_T, and the Temkin isotherm itself is defined by the parameter β_T. A detailed explanation of the β_T parameter shows physical or chemical adsorption if $\beta_T < 8$ kJ/mol and $\beta_T > 8$ kJ/mol, respectively.

2.5.4 Dubinin-Radushkevich

Adsorption involving the process of filling the surface pores of the adsorbent with adsorbate is explained by this isotherm model. Because the adsorption mechanism involves pore filling, the adsorbent surface is predicted to have a heterogeneous surface. According to this model, the size of the adsorbent is proportional to the size of the micropores. The Dubinin-Radushkevich adsorption equation is shown in Equation (5).

$$lnqe = lnqs - \beta\varepsilon^2 \quad (5)$$

In the context of the Dubinin-Radushkevich isotherm, β represents the isotherm constant, $\mathcal{E}$ corresponds to the Polanyi potential relative to the given conditions, and q_s stands for the theoretical saturation capacity (measured in mg/g). The Polanyi potential and the calculation of adsorption energy are provided in Equations (6) and (7), respectively.

$$\varepsilon = RT \ln\left[1 + \frac{1}{Ce}\right] \quad (6)$$

$$E = \frac{1}{\sqrt{2\beta}} \quad (7)$$

where E symbolizes the adsorption energy, indicating the free energy of sorption (expressed in kJ/mol) linked to the movement of individual sorbate molecules from the bulk solution to the solid surface involving physical or chemical process if $E < 8$ kJ/mol and $E > 8$ kJ/mol.

2.5.5 Flory-Huggins

The Flory-Huggins isotherm addresses the degree of adsorbate surface coverage on the adsorbent. Equation (8) provides the formula for calculating the Flory-Huggins Isotherm model.

$$\log\frac{\theta}{C_e} = \log K_{FH} + n\log(1 - \theta) \quad (8)$$

The Flory-Huggins isotherm model is utilized to elucidate the viability and spontaneity of the adsorption process, signifying the reduction in the surface coverage degree from the adsorbate to the adsorbent. Here, θ denotes the extent of surface coverage, whereas K_{FH} and n_{FH} stand as the equilibrium constant and adsorption site, respectively. Equation (9) pertains to the equilibrium constant, K_{FH}, which is employed to ascertain the free Gibbs energy of spontaneity.

$$\Delta G° = -RTlnK_{FH} \quad (9)$$

A negative value for ΔG° indicates the spontaneous nature of the adsorption process, which is also influenced by temperature.

2.5.6 Fowler Guggenheim

Lateral interactions between adsorbed molecules that depend on the heat of adsorption which can increase or decrease with changes in loading are described in this isotherm model. When the interaction between adsorbate molecules involves attractive forces, the energy is positive. Meanwhile, when the interaction between adsorbate molecules involves repulsive forces (a reduction in loading occurs), then the energy is negative. Equation (10) provides the linear representation of this model.

$$K_{FG}C_e = \frac{\theta}{1-\theta}\exp\left(\frac{2.\theta.W}{RT}\right) \quad (10)$$

where W signifies the interaction energy (in kJ/mol) among the adsorbed molecules, while C_e represents the equilibrium constant, and K_{FG} corresponds to the Fowler-Guggenheim equilibrium constant. In detail, the W value shows attraction ($W > 0$ kJ/mol), repulsion ($W < 0$ kJ/mol), and no interaction ($W = 0$ kJ/mol) between adsorbed molecules.

2.5.7 Hill-Deboer

This model represents mobile adsorption and bilateral interactions between molecules that have been adsorbed. According to this model, adsorption is a collaborative process where the capacity of one site to capture an adsorbate molecule impacts the potential of other binding sites on the same macromolecule. Equation (11) delineates the linear representation of this model.

$$K_1.C_e = \frac{\theta}{1-\theta}\exp\left(\frac{\theta}{1-\theta} - \frac{K_2\theta}{RT}\right) \quad (11)$$

where K_1 (L/mg) and K_2 (kJ/mol) are the energy constant of contact in the adsorbed molecular and the Hill-de Boer model, respectively. The K_2 value shows attraction ($K_2 > 0$ kJ/mol), repulsion ($K_2 < 0$ kJ/mol), and no interaction ($K_2 = 0$ kJ/mol) between adsorbed molecules.

2.5.8 Jovanovic

The Jovanovic isotherm considers the potential for mechanical contact between the adsorbate and the adsorbent, incorporating the events described in the Langmuir model. The linear representation of this model is detailed in Equation (12).

$$nQe = lnQ_{max} - K_jC_e \quad (12)$$

where Q_e represents the equilibrium adsorbate amount within the adsorbent (measured in mg/g), Q_{max}

signifies the maximum adsorbate uptake, and K_J denotes the Jovanovic constant.

2.5.9 Harkin-Jura

This model explains the adsorption occurring on the adsorbent surfaces as multilayer adsorption due to the heterogeneous pore distribution of the adsorbent. The linear form of this model is described in Equation (13).

$$\frac{1}{q_e^2} = \frac{B_{HJ}}{A_{HJ}} - \left(\frac{1}{A}\right) log C_e \quad (13)$$

The β_{HJ} value is correlated with the specific surface area of the adsorbent, while A_{HJ} represents the constants associated with the Harkin-Jura isotherm.

2.5.10 Halsey

Adsorption by multilayered adsorption processes was evaluated using the Halsey isotherm. The linear form of this model is described in Equation (14).

$$Q_e = \frac{1}{n_H} ln K_H - \left(\frac{1}{n_H}\right) ln C_e \quad (14)$$

where K_H dan n are the Halsey model constants.

2.6 *Kinetic procedure*

Adsorption kinetics describe the rate of absorption that occurs in the adsorbent to the adsorbate. The characteristics of the adsorbent's ability to absorb adsorbate can be seen from the adsorption rate. The adsorption rate can be known from the adsorption rate constant (k) and the reaction order generated from an adsorption kinetics model. The testing stage of the adsorption rate can be done by estimating the reaction order.

Pseudo-first-order in adsorption kinetics is a kinetic model where the apparent rate of adsorption reaction is that of a first-order reaction, even if the real process is more complicated. When it is observed that the concentration of chemicals adsorbed on the adsorbent surface decreases exponentially with time, this model is commonly used. Equation (15) represents pseudo-first-order kinetics.

$$\ln(Q_e - Q_t) = \ln Q_e - k_i t \quad (15)$$

To simulate the adsorption process on the adsorbent surface, a pseudo-second-order kinetic model is applied. In this model, the amount of adsorbate adsorbed on the adsorbent surface which is defined by Equation (16) is assumed to determine the adsorption reaction rate.

$$\frac{t}{Q_t} = \frac{1}{Q_e^2 k_2} + \frac{t}{Q_e} \quad (16)$$

3 Results and Discussion

3.1 *Physicochemical characterization of biochar based on pomegranate peel*

Figure 3 describes the results of an optical microscope of the prepared biochar microparticles. Detailed information for the analysis of microscope photograph images is explained elsewhere [39]. Biochar has a black color with a heterogeneous and irregular surface structure. In general, the particle size was detected in the range of 500–2000 μm.

The present study was focused on building a fundamental understanding of materials through a microscope because the analyzed particles have relatively large particle sizes (around hundreds of microns). Therefore, an optical microscope is sufficient for the analysis of particle morphology and size. However, to confirm the structure of the particles, additional characterization is required, such as a Scanning Electron Microscope (SEM), which will be performed in our future studies.

Figure 4 presents the FTIR results of biochar based on pomegranate peel before and after adsorption. Detailed information for the analysis of FTIR is explained elsewhere [40], [41]. The FTIR spectrum before ammonia adsorption shows that various bands measured at a wide wavelength at 3475 cm^{-1} are attributed to hydroxyl groups (–OH). The observed weak band from 2980 cm^{-1} is attributed to the six-membered lactone ring near 1735 cm^{-1}. The band at about 1604 cm^{-1} is assigned to carboxylates (carboxylic acid salts). The peak at 1460 cm^{-1} can be attributed to organic sulfate groups and the band at wavelength 1240 cm^{-1} is attributed to Aromatic phosphates (P-O-C stretch). The band at 1091 cm^{-1} can be ascribed to primary amine, C-N stretch, and the band at 989 cm^{-1} is ascribed to vinyl C-H out-of-plane bending. Near the peak of 660 cm^{-1} is thought to come from thioethers, CH_3-S-(C-S stretch) while the peak at 600 cm^{-1} is thought to come from aryl disulfides (S-S stretch) [40]. Detailed information regarding the peaks that appeared in the FTIR analysis is shown in Table 4.

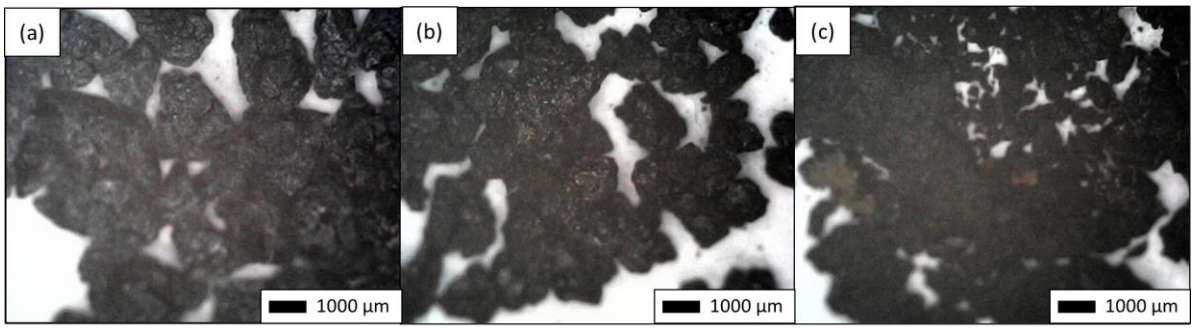

Figure 3: Optical microscope photograph images of biochar: (a) 2000, (b) 1000, and (c) 500 µm.

Table 4: FTIR spectra band assignments for biochar based on pomegranate peels before and after adsorption.

No.	Assignment	Wavelength (cm^{-1})	
		Before Adsorption	After Adsorption
1	O-H stretching of hydroxyl group	3475	3433
2	C-H stretching of methyl group	2980	2860
3	Six-membered ring lactone	1735	-
4	Carboxylate (carboxylic acid salt)	1604	1585
5	Organic sulfates	1460	-
6	Ammonium ion	-	1430
7	Aliphatic nitro compounds	-	1365
8	Aromatic phosphates (P-O-C stretch)	1240	-
9	Secondary amine, CN stretch	-	1190
10	Primary amine, CN stretch	1091	-
11	Aliphatic phosphates (P-O-C stretch)	-	1057
12	Vinyl C-H out-of-plane bend	989	-
13	C-H Monosubstitution (phenyl)	-	770
14	Thioethers, CH_3-S-(C-S stretch)	660	-
15	Aryl disulfides (S-S stretch)	600	-
16	Polysulfides (S-S stretch)	-	513

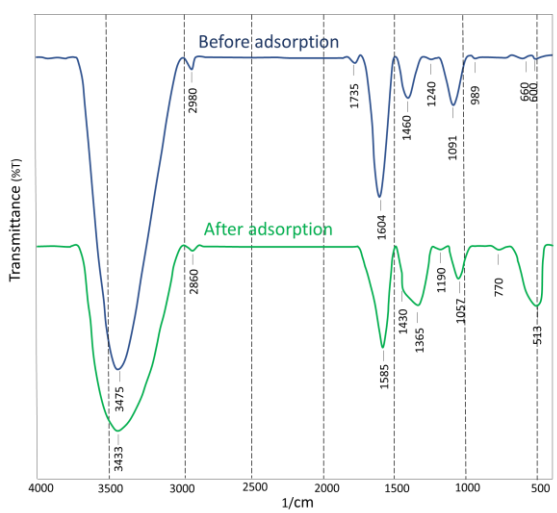

Figure 4: FTIR spectrum of pomegranate peel biochar before and after adsorption.

The presence of peaks for several biochar-based pomegranate peel bands changed after adsorption. The first peak at 3433 cm^{-1} is ascribed to the stretching vibration of O-H on the hydroxyl group and its weakening after adsorption. The C-H stretching groups of the methyl and carboxylic groups (carboxylic acid salts) were observed to experience weak vibrations in the 2860 and 1585 cm^{-1} bands. The six-membered lactone ring identified from the 1735 cm^{-1} band disappeared. However, new FTIR bands were discovered, such as the 1430 cm^{-1} band which was thought to come from ammonium ions and the peak at 1365 cm^{-1} came from aliphatic nitro compounds. The weak bands at 1057, 770, and 513 cm^{-1} come from aliphatic phosphate (P-O-C stretch), C-H monosubstitution (phenyl), and polysulfide (S-S stretch), respectively. Changes in these peaks that occur after adsorption indicate that ammonia (ammonium ion (NH_4^+) has been successfully adsorbed and caused changes in the structure and physical properties of biochar [40].

Thermogravimetric Analysis (TGA) should be done. TGA is effective in understanding how the

material changes after adding heat treatment [42]. This analysis can understand what phenomena happen during additional carbonization for the formation of biochar from biomass. However, since the present study was done to understand the profile of biochar adsorbent in adsorbing ammonia, TGA was not conducted. Further analysis of the TGA for how the biochar is produced from biomass will be done in our future work. Our future work will also analyze to understand the thermal properties of adsorbent materials, including thermal stability and decomposition.

3.2 *Adsorption isotherm model*

The adsorption results of the biochar as an adsorbent made from pomegranate peel were used to understrand the ammonia adsorption equilibrium data compared with ten different isotherm models including Langmuir, Freundlich, Temkin, Dubinin-Radushkevich, Jovanovic, Halsey, Harkin Jura, Flory-Huggins, Fowler-Guggenheim, and Hil-DeBoer models. Table 5 includes an inventory of parameter values and statistical parameters.

Langmuir isotherm represents Equation (1) which explains the lack of identical active sites on the monolayer surface. The Langmuir isotherm model for the three sizes in this investigation exhibited a correlation coefficient (R^2) of more than 0.70, indicating that the equilibrium data suited the Langmuir model. Using the Langmuir model, biochar with diameters of 2000, 1000, and 500 µm had maximum adsorption capacities of 1.263, 1.263, and 1.208 mg/g, respectively. Maximum capacity data shows that larger particle sizes have higher maximum capacity values due to the implication of a porous or macroporous internal structure which offers a large adsorption capacity. Although the particles are large overall, the internal pores provide significant additional surface area. Equation (2) calculates the adsorption behavior (R_L) from the Langmuir model. Table 5 shows that a value of $0 < R_L < 1$ promotes a successful adsorption process [43].

Freundlich isotherm presented in Equation (3), represents the adsorption behavior that occurs on heterogeneous surfaces. Adsorption occurs on heterogeneous surfaces, as evidenced by correlation coefficients (R^2) more than 0.70 for all three adsorbent sizes (2000, 1000, and 500 µm). Table 5 shows adsorption intensity values (n_F) of 1.0183, 0.9174, and 0.1271, respectively. Meanwhile, $1/n$ provides an explanation for the adsorption behavior. According to Table 2, $1/n > 1$ suggests cooperative adsorption [43].

The Temkin isotherm derived with Equation (4), displays the type of energy required at the adsorption active site. Table 5 shows that all adsorption processes for the three sizes (2000, 1000, and 500 µm) exhibit a weak interaction between the adsorbate and adsorbent, generating adsorption chemicals with $\beta_T > 8$ kJ/mol [43].

The Dubinin-Raduskhevich isotherm asserts Equation (5) which describes the mechanism of energy distribution over heterogeneous surfaces. Table 5 shows that the correlation coefficient (R^2) for all three adsorbent sizes (2000, 1000, and 500 µm) is greater than 0.70, indicating the presence of micropores in their surface structure. Equations (6) and (7) were also used to investigate the free energy of adsorption in separating physical and chemical attributes. A value of $E > 8$ kJ implies that a physical process has occurred [43].

Flory-Huggins isotherm describes the creation of heterogeneous adsorbate system layers on the adsorbent surface as indicated in Equation (8). Table 5 shows that all adsorbent sizes have a correlation coefficient (R^2) of greater than 0.70, indicating the formation of a multilayer system. The model investigates the adsorbent molecules' active sites, known as the n_{FH} parameter. Table 5 shows that n_{FH} values < 1 indicate several active molecules in the heterogeneous system [44].

Fowler-Guggenheim isotherm illustrates the influence of lateral molecular interactions between the adsorbent and adsorbed molecules as shown in Equation (10). The parameter W describes the nature of the interaction between adsorbent and adsorbate molecules. Table 5 shows that W parameter values < 0 imply the presence of attractive interactions between particles of all sizes. Furthermore, negative values of the W parameter suggest that the energy conditions between the adsorbate molecules are endothermic [44].

Hill-DeBoer isotherm describes the mobility and mutual interaction of adsorbate molecules. The movement of interactions in this model is examined using Equation (11), denoted by K_2. Table 5 demonstrates that the value $K_2 < 0$ indicates interaction between adsorbate particles of all sizes [45].

Jovanovic isotherm illustrates how the adsorbate and adsorbent interact to produce absorption or desorption. Table 5 shows that a monolayer surface is present at all three adsorbent sizes with a correlation coefficient (R^2) of more than 0.70 [44].

Harkin-Jura depicts the adsorption process, which is analogous to the Freundlich and Halsey isotherms. The calculation results for Equation (13) in Table 5 indicate the same results as those assumed by the Halsey and Freundlich models. Adsorption occurs in a heterogeneous system across all adsorbent sizes as indicated by a correlation coefficient (R^2) value greater than 0.70. This model also explains specific surface area (B_{HJ}). Table 5 shows a positive B_{HJ} value, confirming the association with adsorbent surface area [45].

Halsey isotherm involves a multilayer adsorption mechanism. As indicated in Table 5, a correlation coefficient (R^2) of more than 0.70 confirmed the creation of a multilayer surface throughout the adsorption process [45].

From the previous analysis and explanation of the adsorption isotherm model classified by the correlation coefficient (R^2) value to describe how ammonia adsorption with pomegranate peel biochar of various sizes, the following adsorption isotherm model was found:

1) 2000 μm: Harkin-Jura < Flory-Huggins < Hill-Deboer < Jovanovic < Temkin < Dubinin-Radushkevich < Halsey < Freundlich < Langmuir < Fowler-Guggenheim

2) 1000 μm: Temkin < Flory-Huggins < Dubinin-Radushkevich < Jovanovic < Halsey < Hill-Deboer < Harkin-Jura < Freundlich < Fowler-Guggenheim < Langmuir

3) 500 μm: Fowler-Guggenheim < Flory-Huggins < Jovanovic < Temkin < Halsey < Hill-Deboer < Freundlich < Langmuir < Dubinin-Radushkevich < Harkin Jura

Based on the classification outcomes, the highest correlation coefficient (R^2) signifies the characteristics of pomegranate peel biochar. Our findings reveal that different sizes of pomegranate peel biochar exhibit distinct model fits. Specifically, biochar with a size of 2000 μm shows a notably high correlation coefficient value with the Fowler-Guggenheim model. Conversely, pomegranate biochar measuring 1000 and 500 μm exhibits the highest correlation coefficient values with the Langmuir and Harkin Jura models, respectively. These correlation coefficient values for each biochar size represent the most accurate and predominant fit in elucidating the adsorption capacity of pomegranate peel biochar. In summary, the overall adsorption phenomenon for each particle size is described based on the correlation coefficient (R^2) adjustment results. Under varying conditions, the biochar dose remains constant and only the particle size is considered. We found that large (2000 μm) and medium (1000 μm) biochars showed maximum capacities of 65.631 mg/g and 62.231 mg/g, respectively. For both large and medium-sized biochar (2000 and 1000 μm), the interactions among ammonia molecules indicate repulsive forces and potential lateral interactions on uniformly distributed adsorption sites. Consequently, all adsorption processes on large and medium-sized biochar occur favorably under endothermic conditions, particularly with microporous surfaces. In the context of adsorption, this implies that additional energy is necessary to facilitate the uptake of molecules or particulates [46].

The additional energy that facilitates the adsorption reaction between the adsorbate molecules and the adsorbent surface can come from environmental heat, kinetic energy, radiation, or chemical reactions that occur during the process [46]. This helps to release the adsorbate molecules from the fluid phase and facilitates attachment to the adsorbent surface. Furthermore, the adsorption mechanism for small-sized biochar (500 μm) revealed an adsorption process with favorable distribution pores on homogeneous surface sites with an adsorption capacity of 50.086 mg/g. In addition, the adsorption process on small-sized biochar (500 μm) occurs selectively at low temperatures and endothermic conditions. Thus, additional energy is required to overcome the energy barrier required to release adsorbate molecules from the fluid phase and attach them to the adsorbent surface. A proposal illustration of the adsorption behavior model is shown in Figure 5.

The key finding of this research is that the maximum adsorption capacity is closely related to the size of the biochar particles. Large and medium-sized biochar (2000 and 1000 μm) have a higher adsorption capacity compared to small-sized biochar (500 μm). These findings indicate that increasing the particle size of biochar can increase the ammonia adsorption capacity. In general, particles with a larger surface area (i.e. 500 μm) tend to have a greater adsorption capacity because they have more adsorption sites available to interact with the adsorbate molecules [47], [48]. In this context, large particles have a larger surface area than small particles, because their physical dimensions are larger. Therefore, in many cases, large particles will have a higher maximum adsorption capacity than small particles. Additionally, large particles may have larger or more structurally open shafts, allowing easier access for adsorbate

molecules to attach to the adsorbent surface [49], [50]. This can increase the adsorption capacity significantly. These findings highlight the importance of choosing the right particle size to optimize adsorption efficiency in practical applications.

Apart from that, another key finding from this research is the particle size which influences the adsorption mechanism. Large particles tend to have a higher adsorption capacity due to their larger surface area and more complex pore structure, which allows multilayer adsorption to occur. In contrast, small particles usually show more uniform adsorption interactions on homogeneous sites. However, the use of very small particles may increase the risk of agglomeration or settling, which can reduce adsorption efficiency. Thus, large and medium particles are more effective in adsorption applications due to their ability to diffuse better and increase the adsorption potential of molecules on the particle surface [50].

Table 5: Models of isotherm adsorption in this study.

Model	Parameter	Particle size (µm)			Notes
		2000	1000	500	
Langmuir	R_L	0.2670–1.0000	0.2789–1.0000	0.4834–1.0000	The adsorption is favorable
	Q_{max} ($\frac{mg}{g}$)	65.631	62.231	50.086	The maximum adsorption capacity of the adsorbent
	K_L (L/mg)	0.1841	0.1841	0.1271	The weak interaction between adsorbate and adsorbent is shown by the small value of the Langmuir constant.
	R^2	0.7917	0.9717	0.8274	$R^2 > 0.7$ (monolayer) $R^2 < 0.7$ (multilayer)
Freundlich	$\frac{1}{n_F}$	0.982	1.0900	1.1060	Close to 0, indicating favorable adsorption
	n_F	1.0183	0.9174	0.1271	above 1, shown Physisorption
	R^2	0.7431	0.9097	0.8258	$R^2 > 0.7$ (multilayer) $R^2 < 0.7$ (monolayer)
Temkin	β_T (J/mol)	31.9146	0.817	0.739	Physisorption ($\beta_T > 8$ kJ/mol)
	A_T (L/g)	31.9146	36.3770	45.2368	Temkin equilibrium binding constant
	R^2	0.6794	0.8170	0.7390	$R^2 > 0.7$ (monolayer) $R^2 < 0.7$ (multilayer)
Dubinin-Radushkevich	β (K_{DR})	0.7260	0.8430	0.3760	The constant of the Dubinin-Radushkevich isotherm
	E	0.3580	0.4380	0.3760	Physisorption ($E > 8$ kJ/mol)
	R^2	0.7267	0.8438	0.8309	$R^2 > 0.7$ (pore structure)
Flory-Huggins	n_{FH}	–0.2330	–1.0187	–0.5932	Under 1, the adsorbate takes more than one adsorbent zone
	K_{FH}	0.0071	0.00071	0.0111	The constant of the Flory-Huggins isotherm
Fowler-Guggenheim	K_{FG}	1.4×10^{-58}	8.7×10^{-11}	0.00063081	The constant of the Fowler-Guggenheim isotherm
	W	–1.0205	–32.209	–4.7118	Under 0, interactions between the adsorbed molecules repulsive are endothermic
	R^2	0.93749	0.96358	0.05131	$R^2 > 0.7$ (multilayer) $R^2 < 0.7$ (monolayer)
Hill-Deboer	k_2	–1.145	–4.174	–0.6885	Under 0, interactions between the adsorbed molecules repulsive is endothermic
	R^2	0.62279	0.91379	0.80524	$R^2 > 0.7$ (multilayer) $R^2 < 0.7$ (monolayer)
Jovanovic	K_J	0.668	0.848	0.703	The constant of the Jovanovic isotherm
	Q_{max}	1.15142	1.2080	1.3047	Maximum absorption of adsorbate
	R^2	0.6686	0.8482	0.7037	$R^2 > 0.7$ (monolayer) $R^2 < 0.7$ (multilayer)
Harkin-Jura	A_H	–1.2574	–1.5858	–1.2098	The constant of the Harkin-Jura isotherm.
	B_H	0.0000345	0.0000929	0.00015	Correlated to the surface area of the adsorbent
	R^2	0.04826	0.93849	0.85916	$R^2 > 0.7$ (multilayer)

Model	Parameter	Particle size (μm)			Notes
		2000	1000	500	
					R^2 < 0.7 (monolayer)

Table 5 (*Continued*).

Model	Parameter	Particle size (μm)			Notes
		2000	1000	500	
Halsey	n_H	0.992	0.844	0.607	The isotherm constant of Halsey
	K_H	0.982	1.09	1.106	The constant of the Halsey isotherm
	R^2	0.7431	0.9097	0.8258	R^2 > 0.7 (multilayer)

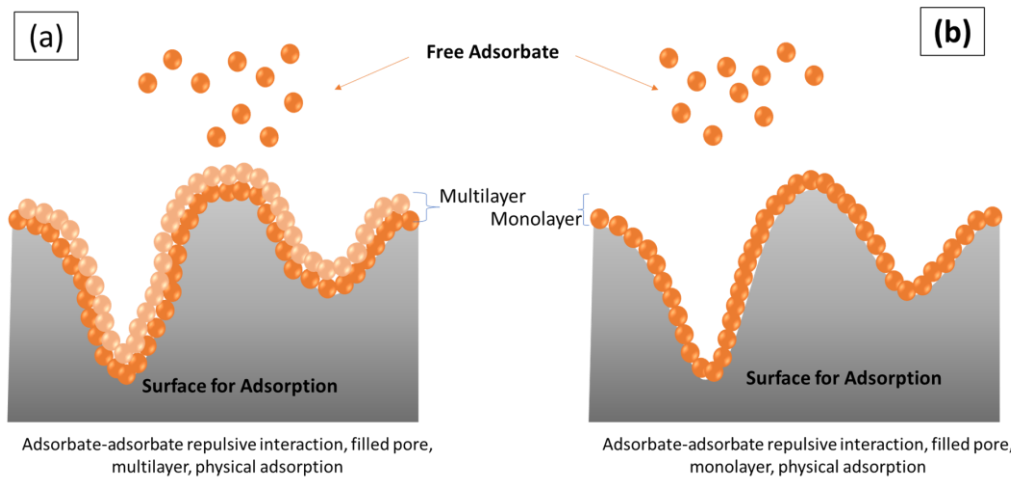

Figure 5: Model of prediction for ammonia adsorption system: (a) 2000 and 1000 μm; (b) 500 μm.

3.3 *Adsorption kinetics*

Table 6 displays the pseudo-first-order and pseudo-second-order parameters that were produced. Kinetic constant parameters and the correlation coefficient (R^2) are employed in kinetics. The pseudo-first-order has a higher correlation coefficient than the pseudo-second-order, according to the data in Table 6. The kinetic constant value shows that the pseudo-first-order has a higher value than the pseudo-second-order. Moreover, ammonia uptake via pseudo-second order has a Q(cal) value that is near to Q(exp), as seen in Table 6. Based on these results, the pseudo-first-order model is very suitable.

3.4 *Proposal adsorption profile*

Overall, the characteristics of the adsorption process for the three sizes show that although adsorption on biochar generally occurs as a single-layer system with interactions between adsorbate molecules on the surface, the uneven distribution of pores in biochar causes a more complex adsorption mechanism. These mechanisms include multi-layer (more than one adsorbate layer) and monolayer (one adsorbate layer) adsorption, as well as various forms of physisorption interactions, which illustrate how biochar pores can be filled with adsorbate molecules in various ways.

This conclusion is supported by pseudo-first-order adsorption process rates, which confirm and provide how the adsorption rate changes over time and often involve monitoring the amount of substance adsorbed over time. In this situation, the adsorption capacity of the biochar adsorbent made from pomegranate peel is greatly influenced by the particle size. The maximum amount of adsorbent that may be adsorbed increases dramatically as the particle size decreases. Nonetheless, as compared to smaller particle sizes, large and medium-sized biochars (1000 μm) were found to function well in this investigation. This happens because the molecules of the material to be adsorbed can diffuse more effectively if medium-sized particles are present. This increased mobility increases the potential for molecules to be adsorbed on the surfaces of large and medium-sized particles.

3.5 *Effect of concentration, adsorbent dosage, and contact time on Isotherm Adsorption*

Adsorption is an important process in many environmental and industrial applications including water treatment. The adsorption process involves the capture of atoms, ions, or molecules from a gas, liquid, or dissolved phase onto a solid or liquid surface. In this study, the adsorption process involves the capture of dissolved molecules onto the surface of a solid. Adsorption efficiency is greatly influenced by various factors, both related to the characteristics of the adsorbent itself and operational conditions [9]. Several factors influence the adsorption process from operational condition factors, including:

Table 6: Ammonia adsorption kinetics over pomegranate peels-based-biochar.

Kinetic	Parameter	Particle Sizes (µm)		
		2000	1000	500
Pseudo first-order model		Q_{exp} = 0.1979		
	R^2	0.9200	0.9209	0.9203
	k_1	3609.80	3898.77	3067.54
	$Q_{(cal)}$	0.2743	1.0653	0.7165
Pseudo order dua model	R^2	0.9015	0.9006	0.9079
	k_2	–0.00017	0.0053	–0.0055
	$Q_{(cal)}$	0.2213	0.2016	0.1998

3.5.1 Concentration

The effect of concentration on the adsorption process is very important because it is directly related to the adsorption capacity and process efficiency. In terms of adsorption capacity, when the concentration of adsorbate in the solution increases there will also be an increase in the number of molecules or ions available to be adsorbed on the surface of the adsorbent. This condition can increase the adsorption capacity to a certain extent because more adsorbates have the potential to interact with the active sites on the adsorbent [51]. Furthermore, with increasing concentration, the active sites on the adsorbent surface become saturated more quickly [52]. In terms of adsorption rate, a higher initial concentration causes a greater concentration gradient between the adsorbate in the solution and on the surface of the adsorbent. Thus, it encourages a faster adsorption rate due to the stronger encouragement of diffusion of adsorbate molecules to the surface of the adsorbent. It also causes opportunities for adsorbate molecules or ions. Interaction between the active site on the adsorbent and adsorbate increases, thereby increasing the adsorption rate, especially in the initial phase of the process [53].

3.5.2 Adsorbent dosage

The higher adsorbent dosage increases the removal amount to a certain limit. After that, it almost approaches constant because when the adsorbent dosage increases, the total number of active sites available for adsorption also increases. Thereby, it increases the efficiency and total adsorption capacity [54]. However, when the adsorbent dosage increases, the adsorption capacity per unit mass usually decreases. This is because increasing the amount of adsorbent offers more active sites. However, it is not always balanced by a sufficient amount of adsorbate to fill all these sites. Furthermore, at very high adsorbent dosage, a decrease in the efficiency per unit mass of the adsorbent may occur due to the phenomenon of agglomeration or accumulation of adsorbent particles, thereby reducing the effective surface area available for adsorption [55].

3.5.3 Contact time

Contact time in adsorption refers to the duration of interaction between the adsorbent (the material used to adsorb) and the adsorbate (the substance being adsorbed). Contact time is a factor that directly influences adsorption efficiency. In the initial stage of adsorption, there is a rapid increase in the amount of adsorbed substance. This is due to the large number of active sites available to be adsorbed on the surface of the adsorbent. Thus, at this stage, only a shorter contact time is needed which is sufficient to reach most of the adsorption capacity [56]. As time goes by, the adsorption rate decreases due to a decrease in the number of available active sites which causes the adsorbate to begin to fill the available sites in the direction of equilibrium [57].

3.6 *Prospect and further research*

After understanding the basic concepts related to adsorption isotherms which analyze the mechanism of contaminant adsorption by the adsorbent surface, discussion regarding the adsorbent recovery process becomes very important. The adsorbent recovery process plays an important role in ensuring efficiency and sustainability. Here, a micrometer-sized biochar-based adsorbent material was used in the wastewater treatment plan because it provides several advantages, especially in terms of effectiveness and ease of recovery of the adsorbent material. It involves relatively easy decantation and filtration procedures. After the adsorption process is completed, the adsorbate solution suspension containing biochar particles can be decanted easily. The biochar particles since has large particle sizes in the micrometer range can be settled easily due to gravity. Then, the liquid above the precipitate, which is ultimately cleaner, can be carefully removed through a decantation process.

Likewise, the filtration process can be carried out to separate micrometer-sized biochar particles that are still suspended in water. The filtration process procedure is to pass the adsorbate solution which still contains biochar particles through a filter media which retains the biochar particles and produces cleaner water. The filters used vary, they can be filter paper, filter cloth, or other filter media that can hold micrometer-sized particles.

The decantation and filtration process is an environmentally friendly recovery process. Recovery of micrometer-sized adsorbents through decantation and filtration processes guarantees the efficiency of the adsorption process for several reasons, especially from the aspect of environmental sustainability, including: 1) the recovery process does not require the use of additional chemicals, thereby reducing negative impacts on the environment; 2) the process does not require significant additional energy thereby reducing energy consumption; and 3) the process is simple and does not require special equipment or high technology thus it is affordable.

Based on the previous perspective, the use of decantation and filtration processes in recovering micrometer-sized biochar adsorbents does not pose or increase risks to the environment and health. In contrast, decantation and filtration processes offer major advantages in terms of environmental sustainability.

3.7 *Limitation*

In this research, we focused on discussing the phenomenon in the context of adsorption isotherms (including adsorption capacity and mechanism) and adsorption kinetics (adsorption rate). However, other intrinsic properties of the adsorbent (such as hydrophilicity/hydrophobicity), stability adsorbent, and swelling characteristics of the adsorbent were not explained. In fact, they are important concepts to discuss due to their influence on the performance of the adsorbent. The hydrophilicity/hydrophobicity aspect does influence adsorption performance.

Then, in the case of stability properties, biochar material is generally considered quite stable (inert) under various operational conditions, including when used in the adsorption process [58]. The stability of biochar in water will greatly depend on the environmental conditions of the water and the presence of certain contaminants or substances in the water, especially if the water contains oxidative species or other reactive species. However, this study used only NH_4Cl as a model adsorbate, in which NH_4Cl is not a highly reactive species in water. NH_4Cl does not react spontaneously or aggressively when dissolved but only dissociates into amine and chloride ions, which are quite stable in solution. Thus, biochar generally exhibits high chemical stability in a variety of solutions, including ammonium chloride solutions.

Biochar indeed has high stability in various solutions. However, biochar adsorbents are susceptible to agglomeration (a process in which small particles aggregate into larger groups) in aqueous media, resulting in a decrease in the effectiveness of the adsorbent. However, hydrophilicity/hydrophobicity and stability aspects have not been discussed in this research and will be carried out in the future.

Furthermore, because we focused on the phenomenon of adsorbate molecules onto the surface of the adsorbent in the adsorption, we did not focus on the efficiency and conditions of the adsorbent, including the swelling ratio. The swelling ratio will be carried out in further research.

3.8 *Contribution to the field of waste management*

This study shows the importance of attention in chemical effluent treatment efforts. In recent years, increased awareness of the negative impact of

chemical effluents on the environment has led to the development of technologies that are more effective in reducing pollution [59]. One prominent solution is the adsorption method applied to adsorb organic pollutants (such as ammonia), which involves the absorption of harmful substances from the waste solution into the adsorbent material. Essentially, this process takes place when the polluting substances adhere to the surface of the adsorbent material, leaving behind a cleaner effluent solution [60]. The production of these organic pollutants has important ecological responsibilities that need to be understood and effectively addressed to maintain environmental balance, especially in industries such as the textile, petrochemical, paper, and pharmaceutical sectors [61].

Many studies highlight the application of this adsorption technique for wastewater treatment due to its ease of operation, ease of regeneration, and minimal side effects [60]. In addition, economic factors that are gaining more attention around the world have increased the attention on adsorption technique as one of the solutions in wastewater treatment [62], [63]. The increasing demand for adsorption techniques has led to demands to improve the stages to make them more effective and efficient. Researchers and engineers are constantly striving to develop more robust and efficient adsorbent materials, as well as optimize operational conditions to improve the performance of adsorption processes.

The main contribution of the adsorption method lies in its ability to remove various types of contaminants from chemical wastes with a high degree of efficiency. By using suitable adsorbent materials, such as activated carbon, zeolite, or biochar, the method can adsorb toxic compounds, heavy metals, and other organic substances from the effluent solution. Thus, continued research in adsorption methods is expected to continue strengthening its contribution to chemical waste treatment. Through collaborative efforts between scientists, engineers, and industries, this method has great potential to become one of the key pillars in global efforts to safeguard the environment and minimize the negative impacts of chemical waste on ecosystems and human health.

4 Conclusions

The present study used pomegranate peel waste as a raw material for preparing biochar microparticles, which was successfully used for removing ammonium molecules. Although adsorption on biochar typically occurs as a single-layer system with interactions between adsorbate molecules on the surface, the uneven distribution of pores in biochar results in a more complex adsorption mechanism. These mechanisms include multi-layer (more than one adsorbate layer) and monolayer (one adsorbate layer) adsorption, as well as various types of physisorption interactions, which demonstrate how biochar pores can be filled with adsorbate molecules in different ways. Here, larger particle sizes have higher maximum capacity values due to the presence of a porous or macroporous internal structure that allows for a high adsorption capacity. Adsorption kinetic analysis revealed that the adsorption process used a pseudo-first-order kinetic model, indicating that the adsorption mechanism was regulated by intraparticle diffusion. As a low-cost adsorbent, the resultant biochar can be effectively utilized for a variety of environmental applications, including the removal of hazardous substances from waste and industrial effluent.

Acknowledgments

We acknowledged the grant “Penelitian Fundamental” from DRPTM DIKTI.

Author Contributions

A.B.D.N.: conceptualization, investigation, reviewing editing, funding acquisition, project administration; A.E.P., M.L., and R.R.: investigation, methodology, writing an original draft; T.K.: research design, data analysis; All authors have read and agreed to the published version of the manuscript

Conflicts of Interest

The authors declare no conflict of interest.

References

[1] T. Ambaye, M. Vaccari, E. D. van Hullebusch, A. Amrane, and S. Rtimi, “Mechanisms and adsorption capacities of biochar for the removal of organic and inorganic pollutants from industrial wastewater,” *International Journal of Environmental Science and Technology*, vol. 18, no. 10, pp. 3273–3294, 2021, doi: 10.1007/s13762-020-03060-w.

[2] A. El-Naggar, S. X. Chang, Y. Cai, Y. H. Lee, J. Wang, S.-L. Wang, C. Ryu, J. Rinklebe, and Y. S. Ok, “Mechanistic insights into the (im)

mobilization of arsenic, cadmium, lead, and zinc in a multi-contaminated soil treated with different biochars," *Environment International*, vol. 156, no. 10, 2021, Art. no. 106638, doi: 10.1016/j.envint.2021.106638.

[3] F. Jing, C. Chen, X. Chen, W. Liu, X. Wen, S. Hu, Z. Yang, B. Guo, Y. Xu, and Q. Yu, "Effects of wheat straw derived biochar on cadmium availability in a paddy soil and its accumulation in rice," *Environmental Pollution*, vol. 257, no. 10, 2020, Art. no. 113592, doi: 10.1016/j.envpol.2019.113592.

[4] B. Liu, T. Chen, B. Wang, S. Zhou, Z. Zhang, Y. Li, X. Pan, and N. Wang, "Enhanced removal of Cd^{2+} from water by AHP-pretreated biochar: Adsorption performance and mechanism," *Journal of Hazardous Materials*, vol. 438, no. 10, 2022, Art. no. 129467, doi: 10.1016/j.jhazmat.2022.129467.

[5] K. R. Parmar and A. B. Ross, "Integration of hydrothermal carbonisation with anaerobic digestion; Opportunities for valorisation of digestate," *Energies*, vol. 12, no. 9, 2019, Art. no. 1586, doi: 10.3390/en12091586.

[6] M. K. Hossain, V. Strezov, K. Y. Chan, A. Ziolkowski, and P. F. Nelson, "Influence of pyrolysis temperature on production and nutrient properties of wastewater sludge biochar," *Journal of Environmental Management*, vol. 92, no. 1, pp. 223–228, 2011, doi: 10.1016/j.jenvman.2010.09.008.

[7] T.-B. Nguyen, Q.-M. Truong, C.-W. Chen, W.-H. Chen, and C.-D. Dong, "Pyrolysis of marine algae for biochar production for adsorption of Ciprofloxacin from aqueous solutions," *Bioresource Technology*, vol. 351, 2022, Art. no. 127043, doi: 10.1016/j.biortech.2022.127043.

[8] M. Sbizzaro, S. C. Sampaio, R. R. dos Reis, F. de Assis Beraldi, D. M. Rosa, C. M. B. de Freitas Maia, C. T. do Nascimento, E. A. da Silva, and C. E. Borba, "Effect of production temperature in biochar properties from bamboo culm and its influences on atrazine adsorption from aqueous systems," *Journal of Molecular Liquids*, vol. 343, 2021, Art. no. 117667, doi: 10.1016/j.molliq.2021.117667.

[9] G. Qi, Z. Pan, X. Zhang, S. Chang, H. Wang, M. Wang, W. Xiang, and B. Gao, "Microwave biochar produced with activated carbon catalyst: Characterization and adsorption of heavy metals," *Environmental Research*, vol. 216, 2023, Art. no. 114732, doi: 10.1016/j.envres.2022.114732.

[10] W. Ahmed, S. Mehmood, A. Núñez-Delgado, S. Ali, M. Qaswar, A. Shakoor, M. Mahmood, and D.-Y. Chen, "Enhanced adsorption of aqueous Pb (II) by modified biochar produced through pyrolysis of watermelon seeds," *Science of The Total Environment*, vol. 784, 2021, Art. no. 147136, doi: 10.1016/j.scitotenv.2021.147136.

[11] W. Lian, L. Yang, S. Joseph, W. Shi, R. Bian, J. Zheng, L. Li, S. Shan, and G. Pan, "Utilization of biochar produced from invasive plant species to efficiently adsorb Cd (II) and Pb (II)," *Bioresource Technology*, vol. 317, 2020, Art. no. 124011, doi: 10.1016/j.biortech.2020.124011.

[12] M. Salimi, Z. Salehi, H. Heidari, and F. Vahabzadeh, "Production of activated biochar from *Luffa cylindrica* and its application for adsorption of 4-Nitrophenol," *Journal of Environmental Chemical Engineering*, vol. 9, no. 4, 2021, Art. no. 105403, doi: 10.1016/j.jece.2021.105403.

[13] Q. Jin, Z. Wang, Y. Feng, Y.-T. Kim, A. C. Stewart, S. F. O'Keefe, A. P. Neilson, Z. He, and H. Huang, "Grape pomace and its secondary waste management: Biochar production for a broad range of lead (Pb) removal from water," *Environmental Research*, vol. 186, 2020, Art. no. 109442, doi: 10.1016/j.envres.2020.109442.

[14] P. A. da Silva Veiga, J. Schultz, T. T. da Silva Matos, M. R. Fornari, T. G. Costa, L. Meurer, and A. S. Mangrich, "Production of high-performance biochar using a simple and low-cost method: Optimization of pyrolysis parameters and evaluation for water treatment," *Journal of Analytical and Applied Pyrolysis*, vol. 148, 2020, Art. no. 104823, doi: 10.1016/j.jaap.2020.104823.

[15] D. F. Al Husaeni, and A. B. D. Nandiyanto, "Bibliometric using Vosviewer with Publish or Perish (using google scholar data): From step-by-step processing for users to the practical examples in the analysis of digital learning articles in pre and post Covid-19 pandemic," *ASEAN Journal of Science and Engineering*, vol. 2, no. 1, pp. 19–46, 2022.

[16] A. B. D. Nandiyanto, M. Fiandini, D. A. Fadiah, P. A. Muktakin, R. Ragadhita, W. C. Nugraha, T. Kurniawan, M. R. Bilad, J. Yunas, and A. S. M. Al Obaidi, "Sustainable biochar carbon microparticles based on mangosteen peel as biosorbent for dye removal: Theoretical review, modelling, and adsorption isotherm characteristics," *Journal of Advanced Research in Fluid*

Mechanics and Thermal Sciences, vol. 105, no. 1, pp. 41–58, 2023, doi: 10.37934/arfmts.105.1.4158.

[17] A. B. D. Nandiyanto, W. C. Nugraha, I. Yustia, R. Ragadhita, M. Fiandini, M. Saleh, and D. R. Ningwulan, "Rice husk for adsorbing dyes in wastewater: literature review of agricultural waste adsorbent, preparation of Rice husk particles, particle size on adsorption characteristics with mechanism and adsorption isotherm," *Journal of Advanced Research in Applied Mechanics*, vol. 106, no. 1, pp. 1–13, 2023, doi: 10.37934/aram.106.1.113.

[18] A. B. D. Nandiyanto, M. Fiandini, R. Ragadhita, H. Maulani, M. Nurbaiti, A. S. M. Al-Obaidi, J. Yunas, and M. R. Bilad, "Sustainable biochar carbon biosorbent based on tamarind (*Tamarindusindica* L) seed: Literature review, preparation, and adsorption isotherm," *Journal of Advanced Research in Applied Sciences and Engineering Technology*, vol. 32, no. 1, pp. 210–226, 2023, doi: 10.37934/araset.32.1.210226.

[19] A. B. D. Nandiyanto, M. Fiandini, R. Ragadhita, R. Maryanti, D. Al Husaeni, and D. Al Husaeni, "Removal of curcumin dyes from aqueous solutions using carbon microparticles from jackfruit seeds by batch adsorption experiment," *Journal of Engineering Science and Technology*, vol. 18, no. 1, pp. 653–670, 2023.

[20] A. B. D. Nandiyanto, D. Al Husaeni, R. Ragadhita, M. Fiandini, R. Maryanti, and D. Al Husaeni, "Computational calculation of adsorption isotherm characteristics of carbon microparticles prepared from mango seed waste to support sustainable development goals (SDGS)," *Journal of Engineering Science and Technology*, vol. 18, no. 2, pp. 913–930, 2023.

[21] A. B. D. Nandiyanto, D. Al Husaeni, R. Ragadhita, M. Fiandini, D. Al Husaeni, and R. Maryanti, "Analysis of adsorption isotherm characteristics for removing curcumin dyes from aqueous solutions using avocado seed waste carbon microparticles accompanied by computational calculations," *Journal of Engingeering, Science and Technology*, vol. 18, no. 1, pp. 706–720, 2023.

[22] A. B. D. Nandiyanto, R. Ragadhita, R. Maryanti, and M. Fiandini, "Curcumin dye adsorption in aqueous solution by carbon-based date palm seed: Preparation, characterization, and isotherm adsorption," *Journal of Applied Research and Technology*, vol. 21, no. 5, pp. 808–824, 2023, doi: 10.22201/icat.24486736e.2023.21.5.1972.

[23] R. Ragadhita, A. Amalliya, S. Nuryani, M. Fiandini, A. Nandiyanto, A. Hufad, A. Mudzakir, W. C. Nugraha, O. Farobie, and I. Istadi, "Sustainable carbon-based biosorbent particles from papaya seed waste: Preparation and adsorption isotherm," *Moroccan Journal of Chemistry*, vol. 11, no. 2, pp. 2395–2410, 2023, doi: 10.48317/IMIST.PRSM/morjchem-v11i2.38263.

[24] A. B. D. Nandiyanto, "Isotherm adsorption of carbon microparticles prepared from pumpkin (*Cucurbita maxima*) seeds using two-parameter monolayer adsorption models and equations," *Moroccan Journal of Chemistry*, vol. 8, no. 3, pp. 2745–2761, 2020.

[25] A. B. D. Nandiyanto, G. C. S. Girsang, R. Maryanti, R. Ragadhita, S. Anggraeni, F. M. Fauzi, P. Sakinah, A. P. Astuti, D. Usdiyana, and M. Fiandini, "Isotherm adsorption characteristics of carbon microparticles prepared from pineapple peel waste," *Communications in Science and Technology*, vol. 5, no. 1, pp. 31–39, 2020, doi: 10.21924/cst.5.1.2020.176.

[26] Y. Mo, J. Ma, W. Gao, L. Zhang, J. Li, J. Li, and J. Zang, "Pomegranate peel as a source of bioactive compounds: A mini review on their physiological functions," *Frontiers in Nutrition*, vol. 9, 2022, Art. no. 887113, doi: 10.3389/fnut.2022.887113.

[27] F. T. Gemeda, D. D. Guta, F. S. Wakjira, and G. Gebresenbet, "Physicochemical characterization of effluents from industries in Sabata town of Ethiopia," *Heliyon*, vol. 6, no. 8, 2020, doi: 10.1016/j.heliyon.2020.e04624.

[28] M. Ilyas, W. Ahmad, H. Khan, S. Yousaf, M. Yasir, and A. Khan, "Environmental and health impacts of industrial wastewater effluents in Pakistan: A review," *Reviews on Environmental Health*, vol. 34, no. 2, pp. 171–186, 2019.

[29] K. Sathya, K. Nagarajan, G. C. G. Malar, S. Rajalakshmi, and P. Raja Lakshmi, "A comprehensive review on comparison among effluent treatment methods and modern methods of treatment of industrial wastewater effluent from different sources," *Applied Water Science*, vol. 12, no. 4, p. 70, 2022, doi: 10.1007/s13201-022-01594-7.

[30] S. Ding, S. F. Dan, Y. Liu, J. He, D. Zhu, and L. Jiao, "Importance of ammonia nitrogen potentially released from sediments to the development of eutrophication in a plateau lake," *Environmental pollution*, vol. 305, 2022, Art. no. 119275, doi: 10.1016/j.envpol.2022.119275.

[31] G. Salbitani, and S. Carfagna, "Ammonium utilization in microalgae: A sustainable method for wastewater treatment," *Sustainability*, vol. 13, no. 2, p. 956, 2021, doi: 10.3390/su13020956.

[32] R. Mishra, "The effect of eutrophication on drinking water," *British Journal of Multidisciplinary and Advanced Studies*, vol. 4, no. 1, pp. 7–20, 2023, doi: 10.37745/bjmas.2022.0096.

[33] K. W. Gemil, D. S. Na'ila, N. Z. Ardila, and Z. U. Sarahah, "The relationship of vocational education skills in agribusiness processing agricultural products in achieving sustainable development goals (SDGs)," *ASEAN Journal of Science and Engineering Education*, vol. 4, no. 2, pp. 181–192, 2024, doi: 10.1111/j.1475-1327. 2024.0244.

[34] M. R. I. Haq, D. V. Nurhaliza, L. N. Rahmat, and R. N. A. Ruchiat, "The influence of environmentally friendly packaging on consumer interest in implementing zero waste in the food industry to meet sustainable development goals (SDGs) needs," *ASEAN Journal of Economic and Economic Education*, vol. 3, no. 2, pp. 111–116, 2024, doi: 10.1234/ ajee.2024.0111.

[35] S. O. Makinde, Y. A. Ajani, and M. R. Abdulrahman, "Smart learning as transformative impact of technology: A paradigm for accomplishing sustainable development goals (SDGs) in education," *Indonesian Journal of Educational Research and Technology*, vol. 4, no. 3, pp. 213–224, 2023, doi: 10.5678/ijert. 2023.0213.

[36] A. B. D. Nandiyanto, R. Andika, M. Aziz, and L. S. Riza, "Working volume and milling time on the product size/morphology, product yield, and electricity consumption in the ball-milling process of organic material," *Indonesian Journal of Science and Technology*, vol. 3, no. 2, pp. 82–94, 2018 doi: 10.7890/ijst.2018.0082.

[37] A. B. Nandiyanto, W. C. Nugraha, I. Yustia, R. Ragadhita, M. Fiandini, H. Meirinawati, and D. R. Wulan, "Isotherm and kinetic adsorption of rice husk particles as a model adsorbent for solving issues in the sustainable gold mining environment from mercury leaching," *Journal of Mining Institute*, vol. 265, pp. 104–120, 2024, doi: 10.5432/jmi.2024.0104.

[38] R. Ragadhita and A. B. D. Nandiyanto, "How to calculate adsorption isotherms of particles using two-parameter monolayer adsorption models and equations," *Indonesian Journal of Science and Technology*, vol. 6, no. 1, pp. 205–234, 2021, doi: 10.7890/ijst.2021.0205.

[39] Y. D. Yolanda, and A. B. D. Nandiyanto, "How to read and calculate diameter size from electron microscopy images," *ASEAN Journal of Science and Engineering Education*, vol. 2, no. 1, pp. 11–36, 2022, doi: 10.1111/ajsee.2022.0011.

[40] A. B. D. Nandiyanto, R. Ragadhita, and M. Fiandini, "Interpretation of Fourier Transform Infrared Spectra (FTIR): A practical approach in the polymer/plastic thermal decomposition," *Indonesian Journal of Science and Technology*, vol. 8, no. 1, pp. 113–126, 2023, doi: 10.7890/ ijst.2023.0113.

[41] S. Sukamto and A. Rahmat, "Evaluation of FTIR, macro and micronutrients of compost from black soldier fly residual: In context of its use as fertilizer," *ASEAN Journal of Science and Engineering*, vol. 3, no. 1, pp. 21–30, 2023, doi: 10.1111/ajse.2023.0021.

[42] R. Ragadhita and A. B. D. Nandiyanto, "Why 200 °C is effective for creating carbon from organic waste (from thermal gravity (TG-DTA) perspective)?," *ASEAN Journal for Science and Engineering in Materials*, vol. 2, no. 2, pp. 75–80, 2022, doi: 10.1111/ajsem.2022.0075.

[43] D. Balarak, F. Mostafapour, H. Azarpira, and A. Joghataei, "Langmuir, Freundlich, Temkin and Dubinin–radushkevich isotherms studies of equilibrium sorption of ampicilin unto montmorillonite nanoparticles," *Journal of Pharmaceutical Research International*, vol. 20, no. 2, pp. 1–9, 2017, doi: 10.9734/jpri/2017/35000.

[44] A. O. Dada, J. Ojediran, A. A. Okunola, F. Dada, A. Lawal, A. Olalekan, and O. Dada, "Modeling of biosorption of Pb (II) and Zn (II) ions onto PaMRH: Langmuir, Freundlich, Temkin, Dubinin-Raduskevich, Jovanovic, Flory-Huggins, Fowler-Guggenheim and Kiselev comparative isotherm studies," *International Journal of Mechanical Engineering and Technology (IJMET)*, vol. 10, no. 2, pp. 1048–1058, 2019, doi: 10.26410/ijmet.2019.1048.

[45] T. Kameda, S. Ito, and T. Yoshioka, "Kinetic and equilibrium studies of urea adsorption onto activated carbon: Adsorption mechanism," *Journal of Dispersion Science and Technology*, vol. 38, no. 7, pp. 1063–1066, 2017, doi: 10.1080/01932691.2017.1294069.

[46] A. Hashem, A. Fletcher, H. Younis, H. Mauof, and A. Abou-Okeil, "Adsorption of Pb (II) ions from contaminated water by 1, 2, 3, 4-

butanetetracarboxylic acid-modified microcrystalline cellulose: Isotherms, kinetics, and thermodynamic studies," *International Journal of Biological Macromolecules*, vol. 164, pp. 3193–3203, 2020, doi: 10.1016/j.ijbiomac.2020.08.217.

[47] C. Wu, M. J. Klemes, B. Trang, W. R. Dichtel, and D. E. Helbling, "Exploring the factors that influence the adsorption of anionic PFAS on conventional and emerging adsorbents in aquatic matrices," *Water Research*, vol. 182, 2020, Art. no. 115950, doi: 10.1016/j.watres.2020.115950.

[48] Y. Cao, M. Zhao, X. Ma, Y. Song, S. Zuo, H. Li, and W. Deng, "A critical review on the interactions of microplastics with heavy metals: Mechanism and their combined effect on organisms and humans," *Science of The Total Environment*, vol. 788, 2021, Art. no. 147620, doi: 10.1016/j.scitotenv.2021.147620.

[49] P. S. Kumar, L. Korving, K. J. Keesman, M. C. van Loosdrecht, and G.-J. Witkamp, "Effect of pore size distribution and particle size of porous metal oxides on phosphate adsorption capacity and kinetics," *Chemical Engineering Journal*, vol. 358, pp. 160–169, 2019, doi: 10.1016/j.cej.2018.09.092.

[50] P. V. Mane, R. M. Rego, P. L. Yap, D. Losic, and M. D. Kurkuri, "Unveiling cutting-edge advances in high surface area porous materials for the efficient removal of toxic metal ions from water," *Progress in Materials Science*, vol. 146, 2024, Art. no. 101314, doi: 10.1016/j.pmatsci. 2023.101314.

[51] T. K. Sen, "Agricultural solid wastes based adsorbent materials in the remediation of heavy metal ions from water and wastewater by adsorption: A review," *Molecules*, vol. 28, no. 14, p. 5575, 2023, doi: 10.3390/molecules28145575.

[52] M. Banerjee, R. K. Basu, and S. K. Das, "Cu (II) removal using green adsorbents: Kinetic modeling and plant scale-up design," *Environmental Science and Pollution Research*, vol. 26, pp. 11542–11557, 2019, doi: 10.1007/ s11356-019-04456-4.

[53] S. Wadhawan, A. Jain, J. Nayyar, and S. K. Mehta, "Role of nanomaterials as adsorbents in heavy metal ion removal from waste water: A review," *Journal of Water Process Engineering*, vol. 33, 2020, Art. no. 101038, doi: 10.1016/ j.jwpe.2019.101038.

[54] S. Jadoun, J. P. Fuentes, B. F. Urbano, and J. Yáñez, "A review on adsorption of heavy metals from wastewater using conducting polymer-based materials," *Journal of Environmental Chemical Engineering*, vol. 11, no. 1, 2023, Art. no. 109226, doi: 10.1016/j.jece.2022.109226.

[55] A. Razzaz, S. Ghorban, L. Hosayni, M. Irani, and M. Aliabadi, "Chitosan nanofibers functionalized by TiO_2 nanoparticles for the removal of heavy metal ions," *Journal of the Taiwan Institute of Chemical Engineers*, vol. 58, pp. 333–343, 2016, doi: 10.1016/j.jtice.2015.06.028.

[56] O. O. Rukayat, M. F. Usman, O. M. Elizabeth, O. O. Abosede, and I. U. Faith, "Kinetic adsorption of heavy metal (Copper) on rubber (*Hevea Brasiliensis*) leaf powder," *South African Journal of Chemical Engineering*, vol. 37, pp. 74–80, 2021, doi: 10.1016/j.sajce.2021.03.002.

[57] O. P. Murphy, M. Vashishtha, P. Palanisamy, and K. V. Kumar, "A review on the adsorption isotherms and design calculations for the optimization of adsorbent mass and contact time," *ACS omega*, vol. 8, no. 20, pp. 17407–17430, 2023, doi: 10.1021/acsomega.2c08058.

[58] M. S. Reza, C. S. Yun, S. Afroze, N. Radenahmad, M. S. A. Bakar, R. Saidur, J. Taweekun, and A. K. Azad, "Preparation of activated carbon from biomass and its' applications in water and gas purification, a review," *Arab Journal of Basic and Applied Sciences*, vol. 27, no. 1, pp. 208–238, 2020, doi: 10.1080/25765299.2020.1729232.

[59] M. T. El-Saadony, A. M. Saad, N. A. El-Wafai, H. E. Abou-Aly, H. M. Salem, S. M. Soliman, T. A. A. El-Mageed, A. S. Elrys, S. Selim, and M. E. A. El-Hack, "Hazardous wastes and management strategies of landfill leachates: A comprehensive review," *Environmental Technology and Innovation*, vol. 31, 2023, Art. no. 103150, doi: 10.1016/j.eti. 2023.103150.

[60] A. J. Tóth, D. Fózer, P. Mizsey, P. S. Varbanov, and J. J. Klemeš, "Physicochemical methods for process wastewater treatment: Powerful tools for circular economy in the chemical industry," *Reviews in Chemical Engineering*, vol. 39, no. 7, pp. 1123–1151, 2023, doi: 10.1515/revce-2021-0094.

[61] F. I. da Silva Aires, D. N. Dari, I. S. Freitas, J. L. da Silva, J. R. de Matos Filho, K. M. dos Santos, V. de Castro Bizerra, M. B. Sales, F. L. de Souza Magalhães, and P. da Silva Sousa, "Advanced and prospects in phenol wastewater treatment technologies: Unveiling opportunities and trends," *Discover Water*, vol. 4, no. 1, pp. 1–36, 2024, doi: 10.1007/s43832-024-00076-y.

[62] R. L. F. Melo, T. M. Freire, R. B. R. Valério, F. S. Neto, V. de Castro Bizerra, B. C. C. Fernandes,

P. G. de Sousa Junior, A. M. da Fonseca, J. M. Soares, and P. B. A. Fechine, "Enhancing biocatalyst performance through immobilization of lipase (Eversa® Transform 2.0) on hybrid amine-epoxy core-shell magnetic nanoparticles," *International Journal of Biological Macromolecules*, vol. 264, no. 2, 2024, Art. no. 130730, doi: 10.1016/j.ijbiomac.2024.130730.

[63] N. S. Rios, E. G. Morais, W. dos Santos Galvão, D. M. A. Neto, J. C. S. Dos Santos, F. Bohn, M. A. Correa, P. B. A. Fechine, R. Fernandez-Lafuente, and L. R. B. Gonçalves, "Further stabilization of lipase from *Pseudomonas fluorescens* immobilized on octyl coated nanoparticles via chemical modification with bifunctional agents," *International Journal of Biological Macromolecules*, vol. 141, pp. 313–324, 2019, doi: 10.1016/j.ijbiomac.2019.09.003.